LETTER

doi:10.1038/nature13893

Agricultural Green Revolution as a driver of increasing atmospheric CO_2 seasonal amplitude

Ning Zeng[1], Fang Zhao[1], George J. Collatz[2], Eugenia Kalnay[1], Ross J. Salawitch[1], Tristram O. West[3] & Luis Guanter[4]

The atmospheric carbon dioxide (CO_2) record displays a prominent seasonal cycle that arises mainly from changes in vegetation growth and the corresponding CO_2 uptake during the boreal spring and summer growing seasons and CO_2 release during the autumn and winter seasons[1–4]. The CO_2 seasonal amplitude has increased over the past five decades, suggesting an increase in Northern Hemisphere biospheric activity[2,5,6]. It has been proposed that vegetation growth may have been stimulated by higher concentrations of CO_2 as well as by warming in recent decades, but such mechanisms have been unable to explain the full range and magnitude of the observed increase in CO_2 seasonal amplitude[2,6–13]. Here we suggest that the intensification of agriculture (the Green Revolution, in which much greater crop yield per unit area was achieved by hybridization, irrigation and fertilization) during the past five decades is a driver of changes in the seasonal characteristics of the global carbon cycle. Our analysis of CO_2 data and atmospheric inversions shows a robust 15 per cent long-term increase in CO_2 seasonal amplitude from 1961 to 2010, punctuated by large decadal and interannual variations. Using a terrestrial carbon cycle model that takes into account high-yield cultivars, fertilizer use and irrigation, we find that the long-term increase in CO_2 seasonal amplitude arises from two major regions: the mid-latitude cropland between 25° N and 60° N and the high-latitude natural vegetation between 50° N and 70° N. The long-term trend of seasonal amplitude increase is 0.311 ± 0.027 per cent per year, of which sensitivity experiments attribute 45, 29 and 26 per cent to land-use change, climate variability and change, and increased productivity due to CO_2 fertilization, respectively. Vegetation growth was earlier by one to two weeks, as measured by the mid-point of vegetation carbon uptake, and took up 0.5 petagrams more carbon in July, the height of the growing season, during 2001–2010 than in 1961–1970, suggesting that human land use and management contribute to seasonal changes in the CO_2 exchange between the biosphere and the atmosphere.

In a 50-year time span from 1961 to 2010, the world population more than doubled, from 3 billion to 7 billion people, while crop production tripled, from 0.5 petagrams of carbon per year (Pg C yr^{-1}) to 1.5 Pg C yr^{-1} (Fig. 1). The threefold increase in crop production was accompanied by a mere 20% increase in the land area of major crops, from 7.2 million km^2 to 8.7 million km^2 (Extended Data Table 1). Higher crop production is thus due mostly to greater yield per unit area, an extraordinary technological feat that is often termed the agricultural Green Revolution. The higher yield can be attributed to three major factors: high-yield crop varieties such as high-yield corn, hybrid dwarf rice and semi-dwarf wheat, use of fertilizer and pesticide, and widespread use of irrigation[14].

The plausibility of a potential Green Revolution impact on the CO_2 seasonal cycle follows from a 'back-of-the-envelope' estimate. The global total terrestrial biosphere net primary productivity (NPP) is about 60 Pg C yr^{-1}, and the seasonal variation from peak to trough is

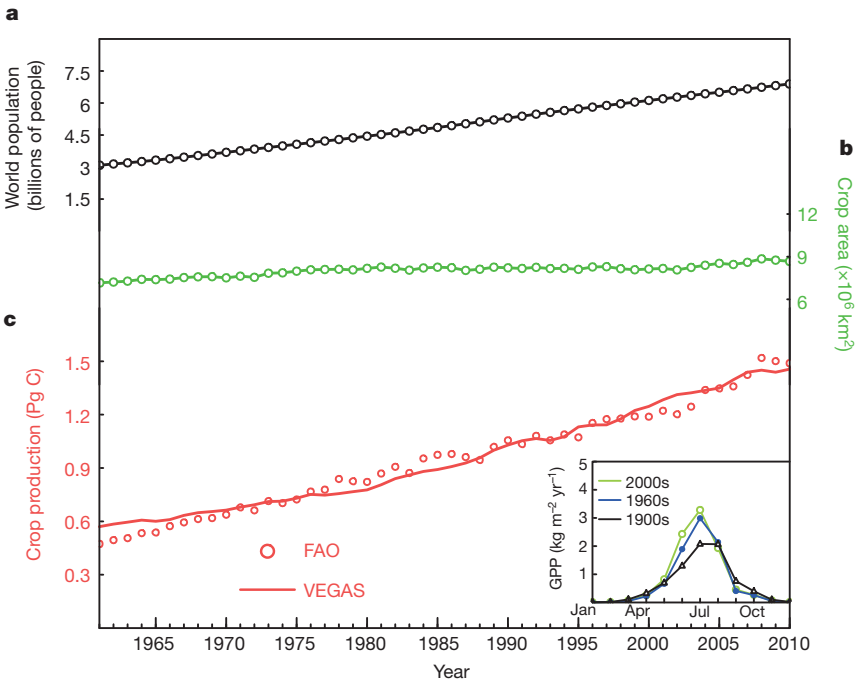

Figure 1 | Changing world population, land area of major crops, annual crop production and changes in crop GPP seasonal cycle. Crop production tripled (**a**) to support 2.5 times more people (**b**) on only 20% more cropland area (**c**), enabled by the agricultural Green Revolution. Plotted in **c** is the VEGAS model simulated crop production, compared to the estimate from FAO statistics. The inset in **c** shows modelled GPP for the periods 1901–1910, 1961–1970 and 2001–2010 for a location in the US Midwest agricultural belt (98° W–40° N) that was initially naturally vegetated and later converted to cropland. The change in seasonal characteristics from these transitions may have contributed to the change in atmospheric CO_2 seasonal amplitude.

[1]Department of Atmospheric and Oceanic Science, and Earth System Science Interdisciplinary Center, University of Maryland, College Park, Maryland 20742, USA. [2]Hydrospheric and Biospheric Sciences, NASA Goddard Space Flight Center, Greenbelt, Maryland 20771, USA. [3]Joint Global Change Research Institute, Pacific Northwest National Laboratory, College Park, Maryland 20740, USA. [4]Institute for Space Sciences, Freie Universität Berlin, 12165 Berlin, Germany.

30–60 Pg C yr^{-1} (ref. 15). Of the NPP, about 6 Pg C yr^{-1} (or 10%) is associated with crop production as the human-appropriated NPP[16–18]. Assuming that half of crop NPP—that is, 3 Pg C yr^{-1}—is the increase due to the Green Revolution, this leads to an increase of global NPP by 5%–10% (3 divided by 60 or 30). This rate is substantial compared to the increase in CO_2 seasonal amplitude[6].

We studied this hypothesis by analysing a variety of observational data and model output, including the Mauna Loa Observatory CO_2 record from 1958 and a global total CO_2 index from 1981 (ref. 3), and atmospheric inversions Jena81 and Jena99[19] and the CarbonTracker[20]. Another key tool is the terrestrial carbon cycle model VEGAS[21,22] which, in a first such attempt, represents the increase in crop gross primary productivity (GPP) by changes in crop management intensity and harvest index (the ratio of grain to total aboveground biomass). Seasonal amplitude is calculated using a standard tool, CCGCRV[23]. Details are in the Methods.

The VEGAS model was run from 1701 to 2010, forced by observed climate, annual mean CO_2, and land-use and management history. The model simulates an increase in crop production from 0.6 Pg C yr^{-1} in 1961 to 1.4 Pg C yr^{-1} in 2010, an increase of 0.8 Pg C yr^{-1}, slightly smaller than the Food and Agriculture Organization of the United Nations (FAO) statistics of 1 Pg C yr^{-1} (Fig. 1). The net terrestrial carbon flux to the atmosphere (the net land–atmosphere carbon flux, F_{TA}) has a minimum in July, corresponding to the highest rate of vegetation growth and carbon uptake (Fig. 2 inset). The maximum of F_{TA} occurs in October, when growth diminishes yet the temperature is still sufficiently warm for high rates of decomposition in the Northern Hemisphere. The model-simulated seasonal cycle of F_{TA}, in both amplitude and phasing, is within the range of uncertainty from the atmospheric inversions (Extended Data Fig. 2).

In the decade of 1961–1970, the average seasonal amplitude of F_{TA} was 36.6 Pg C yr^{-1}. It increased to 41.6 Pg C yr^{-1} during 2001–2010 (Fig. 2 inset). This amplitude increase appears mostly as an earlier and deeper drawdown of CO_2 during the spring/summer growing season. Using −15 Pg C yr^{-1}, which is the mid-point of F_{TA} drawdown, as a threshold, we find that the growing season has lengthened by 14 days, with spring uptake of CO_2 occurring 10 days earlier. The annual mean F_{TA} is −1.6 Pg C yr^{-1} for 2001–2010, implying a net sink whose value is within the uncertainty range from global carbon budget analysis[24]. This mean sink increased over the period, suggesting a relation between seasonal amplitude and the mean sink[6].

The temporal evolution of the seasonal amplitude of F_{TA} exhibits a long-term rise of 15% over 50 years, or 0.3% per year (Fig. 2 and Extended Data Table 2; also see Extended Data Fig. 3 for the detrended monthly time series). There are large decadal and interannual variabilities. The Mauna Loa Observatory CO_2 mixing ratio ($CO2_{MLO}$) shows a similar overall trend but differs from VEGAS on decadal timescales. Most noticeably, a rise in $CO2_{MLO}$ during 1975–1985 precedes a similar rise in VEGAS by several years. This rise was a focus of earlier research[2,7]. A major caveat is that the Mauna Loa Observatory CO_2 data are not directly comparable with modelled F_{TA} because this single station is also influenced by atmospheric circulation, as well as fossil fuel emissions and ocean–atmosphere fluxes. The comparison is nonetheless valuable because the Mauna Loa Observatory data comprise the only long-term record, which is generally considered representative of global mean CO_2 (ref. 5).

We also include in our comparison a global total CO_2 index ($CO2_{GLOBAL}$) and F_{TA} from three atmospheric inversions. The seasonal amplitude of $CO2_{GLOBAL}$, Jena81 and VEGAS are similar but with some differences in the early 1980s (Fig. 2). Otherwise they are similar to VEGAS,

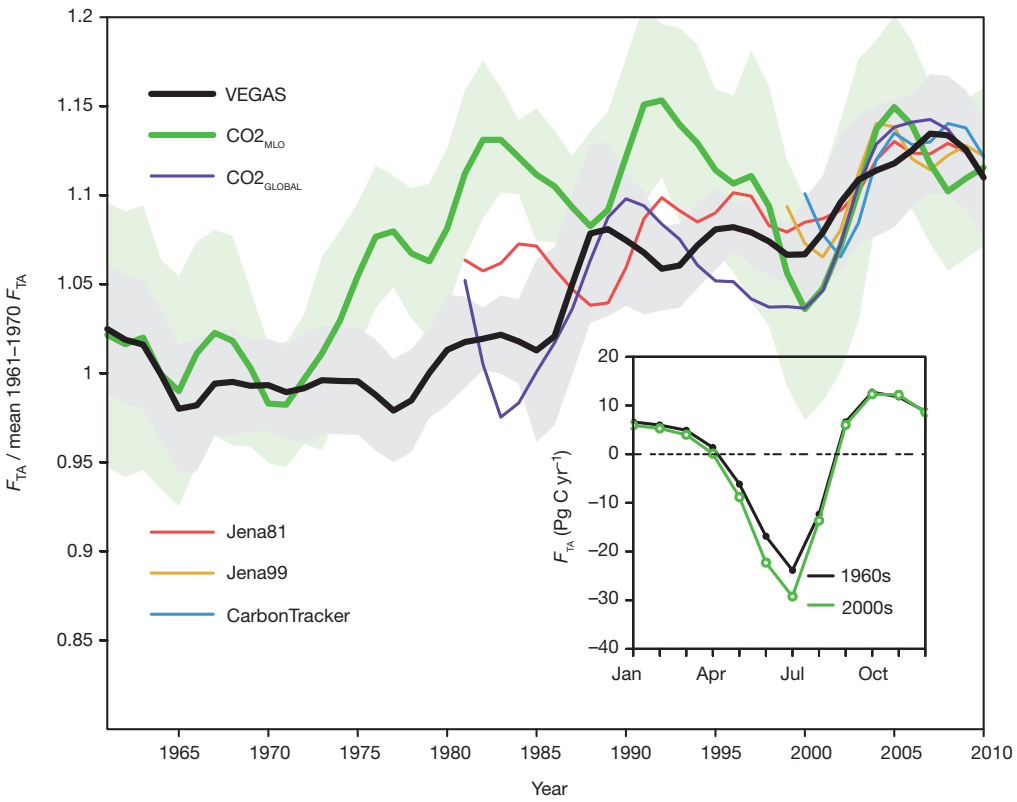

Figure 2 | Temporal evolution of seasonal amplitude. Trends for the VEGAS simulated F_{TA} (black), of the Mauna Loa Observatory CO_2 mixing ratio ($CO2_{MLO}$, green) and the global CO_2 mixing ratio ($CO2_{GLOBAL}$, purple), and F_{TA} from atmospheric inversions of Jena81 (red), Jena99 (brown) and CarbonTracker (blue). Changes are ratios relative to the 1961–1970 mean for VEGAS and the other time series are offset to have the same mean for 2001–2010. Seasonal amplitude is calculated as the difference between the maximum and the minimum of each year after detrending and band-pass filtering with a standard tool, CCGCRV (Extended Data Fig. 3). A 7-year bandpass smoothing removes interannual variability whose 1σ standard deviation is shown for $CO2_{MLO}$ (green shading) and VEGAS F_{TA} (grey shading). The inset shows the average seasonal cycle of VEGAS F_{TA} for the two periods 1961–70 and 2001–2010, showing enhanced CO_2 uptake during the spring/summer growing season.

supporting the above interpretation of local influence in Mauna Loa Observatory CO_2 data[9]. In contrast, if we consider only the period since 1981, Mauna Loa Observatory CO_2 shows little trend because much of the increase occurred earlier, in the 1970s. A decrease in seasonal amplitude in the late 1990s is seen in all data, possibly owing to drought in the Northern Hemisphere mid-latitude regions[9,25]. Similarly, there is consistency in the rapid increase in the first few years of the twenty-first century. In our view, the change in the seasonal CO_2 amplitude is best characterized as a relatively steady long-term increase, modulated by decadal variations, though it can alternatively be viewed as several periods of slow changes or even slight decreases punctuated by large episodic increases.

We further analyse the spatial patterns underlying the seasonal amplitude of F_{TA}. The latitudinal distribution of seasonal amplitude of F_{TA} (Extended Data Fig. 4) shows major contributions from Northern Hemisphere mid-high latitude regions 30° N–70° N, primarily driven by the large seasonal temperature variations there. The two subtropical zones centred at 10° N and 10° S have smaller but distinct seasonal cycles caused by the subtropical wet–dry monsoon-style rainfall changes. The Southern Hemisphere between 40° S and 25° S has a clear seasonal cycle with the opposite sign to that of the Northern Hemisphere, but it is much smaller, owing to its smaller landmass. The atmospheric inversions also depict these broad features, in particular, the major peak in the Northern Hemisphere. VEGAS overestimates the seasonal amplitude between 30° N and 45° N compared to both inversions. Because of seasonal phase differences even within the same hemisphere, the latitudinal distribution does not automatically add up to the global total in the inset to Fig. 2; in particular, the Southern Hemisphere partially cancels out the Northern Hemisphere signal.

Next, we examine the relative contributions of natural vegetation versus cropland in driving the rising seasonal amplitude of F_{TA}. We conducted a similar latitudinal analysis of modelled F_{TA} but separated cropland from natural vegetation, using a cropland mask for the year 2000. The results are shown in Fig. 3. Whereas the seasonal cycle is dominated by natural vegetation at high latitude, cropland is important in the latitude band from 25° N to 60° N, encompassing the world's major agricultural lands of Asia, Europe and North America. Between 35° N and 45° N, the seasonal amplitude of F_{TA} on cropland is even higher than on natural vegetation. In the Southern Hemisphere, there is some contribution from cropland between 20° S and 40° S. A confounding factor is the contemporaneous change in cropland area. However, a sensitivity experiment conducted using the cropland mask of 1961 yielded similar results.

The seasonal amplitude increase between the two time periods 1961–1970 and 2001–2010 is clear both in the naturally vegetated area and in cropland area (Fig. 3). Over cropland, the seasonal amplitude increased nearly everywhere, while a major increase occurred in Northern Hemisphere natural vegetation between 50° N and 70° N. Because the model is forced by the three factors of climate, CO_2 and land-use changes, the seasonal amplitude increase in natural vegetation can come only from climate and CO_2. Between 25° N and 50° N, there is little amplitude change from natural vegetation, suggesting that the combined effect of climate and CO_2 is small there. This could be either because both effects are small, or because climate and CO_2 have opposite impacts that more or less cancel each other out. Because CO_2 fertilization likely enhances NPP and therefore CO_2 amplitude[7], changes in climate may have had a negative impact on the mid-latitude natural vegetation. In contrast, the large F_{TA} seasonal amplitude change seen in cropland area between 35° N and 55° N suggests that land use is responsible there, assuming that crops respond to the combined effect of climate and CO_2 in a way similar to natural vegetation in the same climatic zone. The spatial pattern of the NPP trend (Extended Data Fig. 5) shows the largest increase in the Northern Hemisphere agricultural belts of North America, Europe and Asia, supporting our interpretation that the intensification of agriculture has a key role in F_{TA} seasonal amplitude change.

It may seem surprising that cropland can have such a large impact, because crops are often considered less productive than the natural vegetation they replace, though the opposite may be found for highly productive crops or on irrigated arid land[7,18]. However, for the impact on the CO_2 seasonal cycle, what matters most is that crops have a short but vigorous growing season, leading to a sharper peak and larger seasonal amplitude in GPP (Fig. 1c inset). A sensitivity experiment shows that land-cover change interacts with land management in a non-trivial way (Methods), but the contribution of crops to the increased seasonal amplitude is due mostly to higher crop productivity. Recent space-based measurements of sun-induced fluorescence[26] (SIF) show vividly that at the height of the Northern Hemisphere growing season (July), cropland has the highest productivity, even more than the surrounding dense forests with similar climate conditions (Extended Data Fig. 6), an effect that is broadly captured by VEGAS, but in general not by the other three models analysed.

To further delineate the relative contribution of climate, CO_2 fertilization and land use, we conducted three additional model experiments, termed CLIM, CO2 and LU, respectively. In each experiment, only one of the three forcings is used as model driver, while the other two are fixed. Figure 4 shows the evolution of F_{TA} seasonal amplitude, similar to Fig. 2, but with the fluxes from the three experiments added successively. The sum of the three experiments is similar but not identical to the original simulation (ALL). We calculated the trend to be 0.088% per year for CLIM, 0.076% for CO2, and 0.135% for LU, corresponding to percentage contributions of 29%, 26% and 45% (Extended Data Table 2).

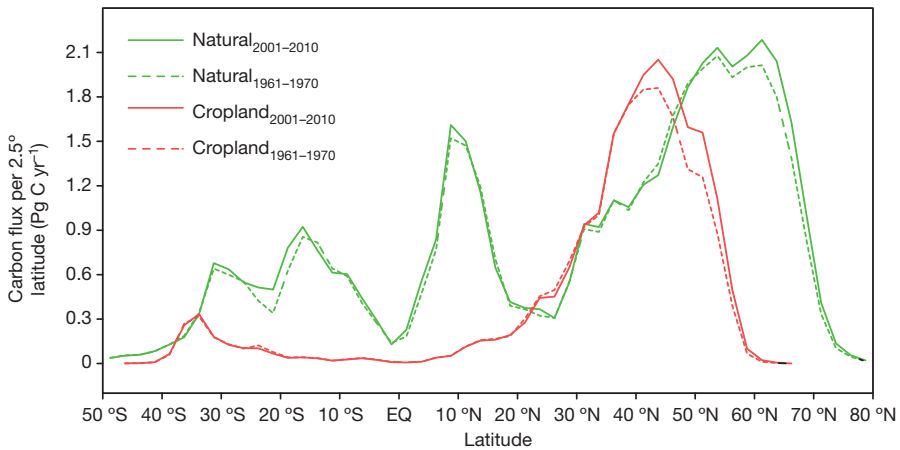

Figure 3 | Latitudinal distribution of the seasonal amplitude of F_{TA}. Calculated separately for natural vegetation (green lines) and cropland (red lines), for the averages of two periods 1961–1970 (dashed) and 2001–2010 (solid).

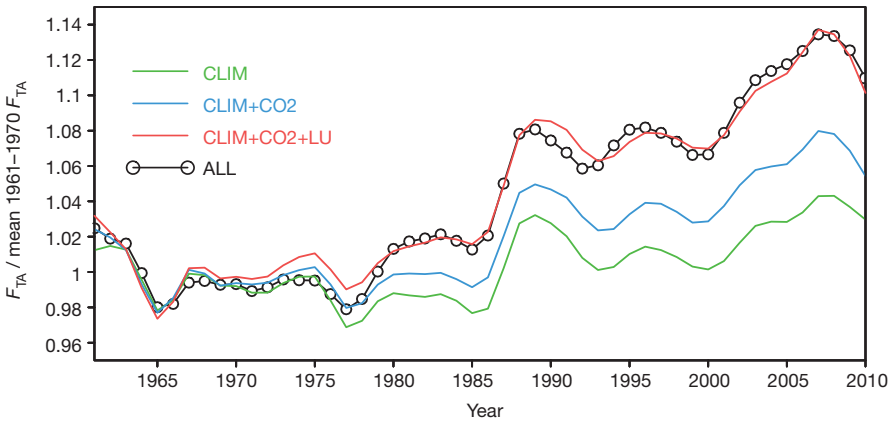

Figure 4 | Attribution of causes with factorial analysis. Relative change of seasonal amplitude from three sensitivity experiments, each with a single forcing: climate only (CLIM, green), CO_2 only (CO2), and land use and management only (LU). The results from CO2 (blue) and LU (red) are added on top of CLIM sequentially. The ALL experiment (black) is the same as in Fig. 2, driven by all three forcings.

The SUM of the three is 0.299% per year, or 3% per decade, or 15% over 50 years. Given uncertainties in the model and data (Methods and Extended Data Fig. 8), the quantitative attribution should be considered merely suggestive. In particular, VEGAS has a CO_2 fertilization strength that is weaker than in some other models that can account for the full amplitude change with fertilization alone[10]. A more challenging task would be to explain spatial patterns better, because models may significantly underestimate the high-latitude trend[12] even if the global total is simulated correctly, the latter being the focus of this paper. Carbon cycle models may have a long way to go in explaining the long-term changes in the seasonal cycle[12], but our results strongly suggest that intensification of agriculture should be included as a driver.

It is generally known that land-use activities such as deforestation and intense agriculture tend to release carbon to the atmosphere, and that recovery from past land clearance sequesters carbon. Our study here suggests yet another aspect of human impact on the global carbon cycle: the basic seasonal characteristics of the biosphere, as indicated by atmospheric CO_2, have been modified by human land-management activities.

Online Content Methods, along with any additional Extended Data display items and Source Data, are available in the online version of the paper; references unique to these sections appear only in the online paper.

Received 6 July 2013; accepted 24 September 2014.

1. Bacastow, R. B., Keeling, C. D. & Whorf, T. P. Seasonal amplitude increase in atmospheric CO_2 concentration at Mauna Loa, Hawaii, 1959–1982. *J. Geophys. Res. D* **90,** 10529–10540 (1985).
2. Keeling, C. D., Chin, J. F. S. & Whorf, T. P. Increased activity of northern vegetation inferred from atmospheric CO_2 measurements. *Nature* **382,** 146–149 (1996).
3. Tans, P. P. & Keeling, R. *Trends in Atmospheric Carbon Dioxide* <http://www.esrl.noaa.gov/gmd/ccgg/trends/> (2013).
4. Tucker, C. J., Fung, I. Y., Keeling, C. D. & Gammon, R. H. Relationship between atmospheric CO_2 variations and a satellite-derived vegetation index. *Nature* **319,** 195–199 (1986).
5. Heimann, M., Keeling, C. D. & Fung, I. Y. in *The Changing Carbon Cycle, a Global Analysis* (eds Trabalka, J. R. & Reichle, D. E.) 16–49 (Springer, 1986).
6. Randerson, J. T., Thompson, M. V., Conway, T. J., Fung, I. Y. & Field, C. B. The contribution of terrestrial sources and sinks to trends in the seasonal cycle of atmospheric carbon dioxide. *Glob. Biogeochem. Cycles* **11,** 535–560 (1997).
7. Kohlmaier, G. H. *et al.* Modelling the seasonal contribution of a CO_2 fertilization effect of the terrestrial vegetation to the amplitude increase in atmospheric CO_2 at Mauna Loa Observatory. *Tellus B* **41,** 487–510 (1989).
8. Myneni, R. B., Keeling, C. D., Tucker, C. J., Asrar, G. & Nemani, R. R. Increased plant growth in the northern high latitudes from 1981 to 1991. *Nature* **386,** 698–702 (1997).
9. Buermann, W. *et al.* The changing carbon cycle at Mauna Loa Observatory. *Proc. Natl Acad. Sci. USA* **104,** 4249–4254 (2007).
10. McGuire, A. D. *et al.* Carbon balance of the terrestrial biosphere in the twentieth century: analyses of CO_2, climate and land use effects with four process-based ecosystem models. *Glob. Biogeochem. Cycles* **15,** 183–206 (2001).
11. Piao, S. *et al.* Evaluation of terrestrial carbon cycle models for their response to climate variability and to CO_2 trends. *Glob. Change Biol.* **19,** 2117–2132 (2013).
12. Graven, H. *et al.* Enhanced seasonal exchange of CO_2 by northern ecosystems since 1960. *Science* **341,** 1085–1089 (2013).
13. Cadule, P. *et al.* Benchmarking coupled climate-carbon models against long-term atmospheric CO_2 measurements. *Glob. Biogeochem. Cycles* **24,** http://dx.doi.org/10.1029/2009gb003556 (2010).
14. Jain, H. K. *The Green Revolution: History, Impact and Future* 1st edn (Studium Press, 2010).
15. Cramer, W. *et al.* Comparing global models of terrestrial net primary productivity (NPP): overview and key results. *Glob. Change Biol.* **5,** 1–15 (1999).
16. Haberl, H. *et al.* Quantifying and mapping the human appropriation of net primary production in Earth's terrestrial ecosystems. *Proc. Natl Acad. Sci. USA* **104,** 12942–12947 (2007).
17. Imhoff, M. L. *et al.* Global patterns in human consumption of net primary production. *Nature* **429,** 870–873 (2004).
18. Vitousek, P. M., Ehrlich, P. R., Ehrlich, A. H. & Matson, P. A. Human appropriation of the products of photosynthesis. *Bioscience* **36,** 368–373 (1986).
19. Rödenbeck, C., Houweling, S., Gloor, M. & Heimann, M. CO_2 flux history 1982–2001 inferred from atmospheric data using a global inversion of atmospheric transport. *Atmos. Chem. Phys.* **3,** 1919–1964 (2003).
20. Peters, W. *et al.* An atmospheric perspective on North American carbon dioxide exchange: CarbonTracker. *Proc. Natl Acad. Sci. USA* **104,** 18925–18930 (2007).
21. Zeng, N. Glacial-interglacial atmospheric CO_2 change—the glacial burial hypothesis. *Adv. Atmos. Sci.* **20,** 677–693 (2003).
22. Zeng, N., Mariotti, A. & Wetzel, P. Terrestrial mechanisms of interannual CO_2 variability. *Glob. Biogeochem. Cycles* **19,** Gb1016, http://dx.doi.org/10.1029/2004GB002273 (2005).
23. Thoning, K. W., Tans, P. P. & Komhyr, W. D. Atmospheric carbon dioxide at Mauna Loa Observatory. 2. Analysis of the NOAA GMCC data, 1974–1985. *J. Geophys. Res. D* **94,** 8549–8565 (1989).
24. Le Quéré, C. *et al.* The global carbon budget 1959–2011. *Earth Syst. Sci. Data* **5,** 165–185 (2013).
25. Zeng, N., Qian, H. F., Roedenbeck, C. & Heimann, M. Impact of 1998–2002 midlatitude drought and warming on terrestrial ecosystem and the global carbon cycle. *Geophys. Res. Lett.* **32,** L22709 (2005).
26. Guanter, L. *et al.* Global and time-resolved monitoring of crop photosynthesis with chlorophyll fluorescence. *Proc. Natl Acad. Sci. USA* **111,** E1327–E1333 (2014).

Acknowledgements We thank all data providers, especially the NOAA CO_2 and CarbonTracker team, and the Jena inversion team. M. Heimann suggested the flux data site comparison. This research was supported by NOAA (NA10OAR4310248 and NA09NES4400006), the NSF (AGS-1129088), and NASA (NNH12AU35I).

Author Contributions N.Z. designed the research and all authors contributed to the ideas. N.Z. and F.Z. conducted the simulations and data analysis. L.G. analysed the TRENDY models and satellite SIF data. N.Z. wrote the paper with input from all others.

Author Information Reprints and permissions information is available at www.nature.com/reprints. The authors declare no competing financial interests. Readers are welcome to comment on the online version of the paper. Correspondence and requests for materials should be addressed to N.Z. (zeng@atmos.umd.edu).

METHODS

Crop production data. Crop production and cropland area is aggregated from FAO statistics for the major crops (FAOSTAT, http://faostat.fao.org/site/567/default.aspx#ancor). Specifically, it is the sum of the cereals (wheat, maize, rice, barley, and so on) and five other major crops (cassava, oil palm, potatoes, soybean and sugarcane), which comprise 90% of the global amount of carbon harvested. Following ref. 27, conversion factors are used to convert the wet biomass to dry biomass, then to carbon content. The final conversion factors from wet biomass to carbon are 0.41 for cereals, 0.57 for oil palm, 0.11 for potatoes, 0.08 for sugarcane, 0.41 for soybean and cassava.

SIF data. SIF data are derived from top-of-atmosphere radiance spectra measured by the Global Ozone Monitoring Experiment-2 (GOME-2) instrument on board the satellite Eumetsat's MetOp-A platform[26]. SIF retrievals are performed in the 715 nm–758 nm spectral window, sampling the second peak of the SIF emission[28]. The retrievals have been quality-filtered, aggregated as monthly averages and gridded globally in half-degree grid boxes. The SIF is thought to be a direct indicator of GPP, though the relationship may be complex[26,29].

Mauna Loa and global mean CO_2 data. Both sets of CO_2 data are from NOAA/ESRL (www.esrl.noaa.gov/gmd/ccgg/trends/). The Mauna Loa Observatory CO_2 record dates back to 1958 but is limited to one single station. The global average is based on multiple marine surface sites, available from 1981, and is constructed by first fitting a smoothed curve as a function of time to each site, and then plotting the smoothed value for each site as a function of latitude for 48 equal time steps per year. A global average is calculated from the latitude plot at each time[23,30].

Atmospheric inversions data. We used CO_2 concentration measurements from a global network of stations and information on atmospheric motion in a transport model to infer the surface CO_2 fluxes. The two inversions from the Max Planck Institute of Biogeochemistry[19] used here are version 3.4 (http://www.bgc-jena.mpg.de/~christian.roedenbeck/download-CO2/), with Jena81 for the period 1981–2010 using CO_2 data from 15 stations, and Jena99 from 61 stations for 1999–2010. The CarbonTracker[20] from NOAA/ESRL is the version CT2011 (http://www.esrl.noaa.gov/gmd/ccgg/carbontracker/), covering 2000–2010, using flask samples from 81 stations, 13 continuous measurement stations and 9 towers. CarbonTracker also uses the surface fluxes from land and ocean carbon models as prior fluxes.

CO_2 and flux seasonal amplitude data. The seasonal amplitude of Mauna Loa Observatory or global CO_2 growth rate and fluxes from model and inversions was calculated as the difference between the maximum and minimum values of each year using high-frequency filtered data with the standard package CCGCRV from NOAA/ESRL (http://www.esrl.noaa.gov/gmd/ccgg/mbl/crvfit/crvfit.html), involving polynomial and harmonic fitting, detrending and band-pass filtering.

Modelling the agricultural Green Revolution. Important progresses have been made in modelling agriculture in global carbon cycle models[31–33]. Such models typically simplify the problem of dealing with multiple crops by using only a handful of crop functional types. Yet this still requires a large number of input data or assumptions on irrigation, crop selection, fertilizer use, planting, harvesting and other management practices that vary widely in space and time. More importantly, there is a general lack of information on historical changes in these driver data and parameter values, so that the temporal changes are not easily represented in such models. Here we adopt a minimalist approach, aiming at capturing the first-order effects relevant to the global carbon cycle with generic rules, thus avoiding the need for unavailable details. Acknowledging its coarse 'precision', to our knowledge, it is a first attempt in global carbon cycle modelling to simulate the intensification of agriculture associated with the Green Revolution. The results are validated using FAO crop production, human-appropriated NPP, satellite measurements of chlorophyll fluorescence and site flux measurements (see the 'Validation of crop simulation' section).

We simulate agriculture with a generic crop functional type that represents an average of the three dominant crops: maize, wheat and rice. The characteristics are in many respects similar to warm C3 grass, one of the natural plant functional types in VEGAS[22]. A major difference is the narrower temperature growth function, to represent a warmer temperature requirement than natural vegetation has. Management of cropland is modelled as an enhanced gross carbon assimilation rate by the human-selected cultivar, application of fertilizers and pesticides, and irrigation. These three factors are thought to have contributed approximately equally to the increase in agricultural productivity over the last half-century[34]. However, the intensity of management varies widely and has not always changed in synchrony in different parts of the world. Instead of using an extensive set of actual management data that are not available or incomplete, we model the first-order effects on carbon cycle by parameterizations with the following rules.

To represent the enhanced productivity from cultivar and fertilization, the gross carbon assimilation rate is modified by a management intensity factor MI that varies spatially and changes over time:

$$\mathrm{MI} = M_0 M_1 \left(1 + 0.2 \tanh\left(\frac{y-2000}{70}\right)\right) \quad (1)$$

where M_1 is the spatially varying component while M_0 is a scaling parameter. M_1 is stronger in temperate and cold regions and weaker in tropical countries, represented here using the annual mean temperature as a surrogate. The term in parentheses is the temporal change (where y is the year), modelled by a hyperbolic tangent function, with parameter values such that in 1961 it was about 10% lower than in 2000, and 20% lower asymptotically far back in time (Extended Data Fig. 1, top panel).

To represent the effect of irrigation, the soil moisture function ($\beta = w_1$ for unmanaged grass, where w_1 is surface soil wetness) is modified as:

$$\beta = 1 - \frac{1 - w_1}{W_{\mathrm{irrg}}} \quad (2)$$

The irrigation intensity W_{irrg} varies spatially from 1 (no irrigation) to 1.5 (high irrigation), corresponding to a β range of 0 (no irrigation) to 0.33 (high irrigation) under extreme dry natural conditions (for extreme desert $w_1 = 0$). This formulation also modifies β when w_1 is not zero, but the effect of irrigation becomes smaller when w_1 increases and has no effect when $w_1 = 1$ (saturated). Thus β (and therefore photosynthesis rate) depends on naturally available water (w_1) as well as irrigation. This is a 'gentler' approach than the assumption of unlimited amount of water on irrigated land, as is sometimes assumed in modelling. The spatial variation in W_{irrg} represents a tropical versus temperate regional difference. Unlike fertilizer/cultivar effects, no temporal changes are assumed because no matter when an area is planted with crops, it must be watered. This assumption may underestimate increased irrigation in some regions, but is the simplest assumption to make in the absence of time-specific data for a given region.

Planting is not prescribed, but allowed whenever the climate condition is suitable (for example, when it is warm enough in temperate and cool regions). This captures much of the spring planting, but misses some other crop types such as winter wheat, which has an earlier growth and harvest—this is a limitation of our simple rule-based approach, which does not use actual regional agricultural practice data. A crop is harvested when it matures, determined by the leaf area index growth rate slowing down to a threshold value. This combination of climate-determined planting and harvest criteria automatically leads to double crops in some warm regions, but it may or may not match actual practice there. Rather, the simulated results only suggest a cropping potential given the characteristics of our generic crop and climate.

After harvest, grain goes into a harvest pool, and the residue is sent to the metabolic carbon pool and decomposes rapidly. A key agricultural advance has been the use of high-yield dwarf cultivars with more edible parts (grain) per unit total biomass, especially since the Green Revolution in the 1960s. This is represented by the harvest index, which is the edible fraction of aboveground biomass. The harvest index varies somewhat for different crops, and we use 0.45 for the year 2000, a value typical of the three major crops: maize, rice and wheat[16,34]. The temporal change is modelled as:

$$\mathrm{HI}_{\mathrm{crop}} = 0.45\left(1 + 0.6 \tanh\left(\frac{y-2000}{70}\right)\right) \quad (3)$$

so that at the beginning of the Green Revolution in 1961 $\mathrm{HI}_{\mathrm{crop}}$ was 0.31, a difference of 0.14 from the 2000 value of 0.45, based on literature values[34]. The parameter values above also imply that $\mathrm{HI}_{\mathrm{crop}} = 0.18$ far back in time ($y = -\infty$), and $\mathrm{HI}_{\mathrm{crop}} = 0.49$ in 2010 (Extended Data Fig. 1, lower panel).

The harvested crop is redistributed according to population density, resulting in the lateral transport of carbon. As a result, there is net carbon uptake in cropland areas and large release of CO_2 in urban areas. To the first-order approximation, the lateral transport is applied within each continent. Additional information on cross-region trade was also implemented for eight major world economic regions.

Validation of crop simulation. There is a general lack of relevant global data on the change in agriculture. We use the FAO global crop production statistics, spanning the period 1961 to the present.

Additionally, we validate the model simulation with estimates of global crop NPP[16], SIF and flux measurement (http://fluxdata.org) at site level. The latter data sets do not offer information on long-term changes, but are useful for validating the model's crop simulation of the present state. Because the model does not use high-spatial-resolution land use and management data such as irrigation, crop type and harvest practices other than land-cover data set (crop/pasture versus natural vegetation from the HYDE data set), small-scale regional patterns may not be well simulated, and the results are more reliable at aggregated continental to global scales.

FAO statistics. Our modelled crop production increased from 0.6 Pg C yr^{-1} in 1961 to 1.4 Pg C yr^{-1} in 2010, somewhat slower than FAO statistics (from 0.5 to 1.5) (Fig. 1 and Extended Data Table 1). The general trends are very similar. FAO statistics has somewhat larger year to year variation, probably due to human factors

influencing crop production other than climate variability, and thus not represented in the model. Note that 'crop production' in the FAO parlance refers only to the edible parts (mostly grain, but also including other parts such as storage organs in potatoes), whereas the total biological NPP on cropland is called NPP_{crop}, including all edible or non-edible biomass above and below ground. Thus NPP_{crop}, not 'crop production', is the quantity that is directly relevant to carbon cycle. The harvest index is needed to relate them.

Human-appropriated NPP. The global total NPP on cropland NPP_{crop} of cropland area is 6.2 Pg C yr^{-1} at 2010, within the range of statistics-based estimate of 6.05-8.18 Pg C yr^{-1} (ref. 16). Such agreement is encouraging given the simplicity in our model representation of agriculture and the uncertainties in the statistics-based estimates. Because of the large increase in harvest index, the modelled 130% increase in crop production corresponds to a smaller increase in NPP_{crop}, from 4 Pg C yr^{-1} in 1961 to 6.2 Pg C yr^{-1} in 2010, which is a 55% increase (Extended Data Table 1).

SIF. We compared remotely sensed chlorophyll fluorescence with four mechanistic carbon cycle models participating in the TRENDY intercomparison project (VEGAS, LPJ, Orchidee, LPJ-Guess), and a data-driven model MPI-BGC, shown in Extended Data Fig. 6. SIF is considered a direct measurement of GPP, as opposed to net carbon flux, thus offering high-resolution global coverage of GPP that is otherwise impractical to obtain with *in situ* methods. While the SIF–GPP relationship may be complex, the spatial pattern can be a particularly meaningful comparison. At the height of a Northern Hemisphere growing season (July 2009), the highest GPPs, according to the satellite fluorescence measurements, were found in the United States and European agricultural regions. Interestingly, three of the four models do not capture this pattern, instead showing the highest GPP values in boreal and partly temperate forest regions. The spatial pattern of VEGAS-modelled GPP agrees reasonably well with satellite fluorescence, perhaps not surprisingly, given that VEGAS is the only model of these four to have a representation of the increased productivity due to the agricultural Green Revolution.

FLUXNET site comparison. We compared the net ecosystem exchange (NEE) and its components GPP and total ecosystem respiration R_e ($NEE = R_e$ minus GPP) at Bondville, Illinois, a no-till maize and soybean site of the AmeriFlux/FLUXNET network (http://www.fluxdata.org:8080/SitePages/siteInfo.aspx?US-Bo1). The results are shown in Extended Data Fig. 7. Model-simulated NEE, GPP and R_e are all in broad agreement with the measurements, with slightly larger seasonal amplitude in NEE. In fact, the level of agreement is somewhat surprising given the simplicity of the model. This may be in part due to the fact that our modelled crop has characteristics that closely match this site. The carbon uptake occurs mostly during the short growing season of June–August, but at a very high rate with maximum GPP of 450 gC m^{-2} in July. This short-duration, high-growth feature can also be seen in Fig. 1 inset, and has contributed noticeably to the increased seasonal amplitude.

Sensitivity experiment on land cover effects. There is a compounding factor of land-cover change (conversions between land-cover types such as cropland and natural vegetation) versus change in land management practices (fertilizer, irrigation and so on). We inferred that the contribution to CO_2 seasonal amplitude trend is dominated by land management because of the threefold increase in crop production compared to the change in cropland area of only 20%. To quantify this conjecture, we conducted an additional model sensitivity experiment in which only land cover is allowed to change but with land management fixed at the 2000 value. The result is that land-cover change alone would decrease the seasonal cycle amplitude of F_{TA} by 0.06% per year, compared to 0.3% per year increase in the ALL experiment (Extended Data Table 2). Thus, the land-cover change effect alone would reduce the trend (with all forcings) by 17% (0.06/(0.3 + 0.06), assuming linearity). This is certainly a nontrivial effect, although the 2000 values for management intensities probably lead to overestimation. The fact that it decreases the seasonal amplitude against the increasing trend may be a bit surprising. This is because the overall increase in cropland area occurred mostly in the tropics while regions north of 30° N have actually decreased in cropland area (owing to a variety of factors such as cropland abandonment, reforestation, urbanization, and so on) where the seasonal cycle is most profound.

Uncertainty analysis. We conducted experiments to assess a 'parametric' uncertainty. We asked how the model-simulated trend in seasonal amplitude would differ if key parameters in management intensity have a given error. We obtained a preliminary version of an FAO-data-based spatially varying crop NPP estimate from T. West. We took the difference between our modelled crop NPP and this observationally based NPP. We then used this difference to infer an 'error bar' for our model parameter uncertainty in management intensity (equation (1) in Methods). We then conducted two simulations to bracket the range of the resulting F_{TA} seasonal amplitude. The results are shown in Extended Data Fig. 8. The resulting trend has an uncertainty range of 0.311% ± 0.027% per year. The relative error in the trend is thus 8.5% (= 0.027/0.311), which is smaller than the uncertainty associated with interannual variability (Fig. 2). This is clearly a very limited way to assess many possible uncertainties, but was the best we could do given the limitations in data availability. Another kind of uncertainty estimate, the standard deviation of the interannual variability in the CO_2 data, was plotted in Fig. 2 as shaded green and grey. Additional models that are capable of representing the intensification of agriculture and relevant observations will be needed for better assessment.

Availability of data and model output. The standard VEGAS model output analysed here is from VEGAS version 2.1, as provided through the international TRENDY project (http://dgvm.ceh.ac.uk) and used in the Global Carbon Project annual carbon budget analysis[24] and the NACP MsTMIP project (http://nacp.ornl.gov/MsTMIP.shtml), downloadable from either site. The model output and the processed data are also available directly from the authors. The use of the data is subject to the policies described in those two sites.

27. Ciais, P., Bousquet, P., Freibauer, A. & Naegler, T. Horizontal displacement of carbon associated with agriculture and its impacts on atmospheric CO_2. *Glob. Biogeochem. Cycles* **21,** (2007).
28. Joiner, J. *et al.* Global monitoring of terrestrial chlorophyll fluorescence from moderate-spectral-resolution near-infrared satellite measurements: methodology, simulations, and application to GOME-2. *Atmospheric Measurement Techniques* **6,** 2803–2823 (2013).
29. Parazoo, N. C. *et al.* Interpreting seasonal changes in the carbon balance of southern Amazonia using measurements of XCO_2 and chlorophyll fluorescence from GOSAT. *Geophys. Res. Lett.* **40,** 2829–2833 (2013).
30. Masarie, K. A. & Tans, P. P. Extension and integration of atmospheric carbon-dioxide data into a globally consistent measurement record. *J. Geophys. Res. D* **100,** 11593–11610 (1995).
31. Bondeau, A. *et al.* Modelling the role of agriculture for the 20th century global terrestrial carbon balance. *Glob. Change Biol.* **13,** 679–706 (2007).
32. Gervois, S. *et al.* Including croplands in a global biosphere model: methodology and evaluation at specific sites. *Earth Interact.* **8,** http://dx.doi.org/10.1175/1087-3562(2004)8<1:ICIAGB>2.0.CO;2 (2004).
33. Kucharik, C. J. & Brye, K. R. Integrated Blosphere Simulator (IBIS) yield and nitrate loss predictions for Wisconsin maize receiving varied amounts of nitrogen fertilizer. *J. Environ. Qual.* **32,** 247–268 (2003).
34. Sinclair, T. R. Historical changes in harvest index and crop nitrogen accumulation. *Crop Sci.* **38,** 638–643 (1998).
35. Jung, M. *et al.* Global patterns of land-atmosphere fluxes of carbon dioxide, latent heat, and sensible heat derived from eddy covariance, satellite, and meteorological observations. *J. Geophys. Res. Biogeosci.* **116,** http://dx.doi.org/10.1029/2010JG001566 (2011).

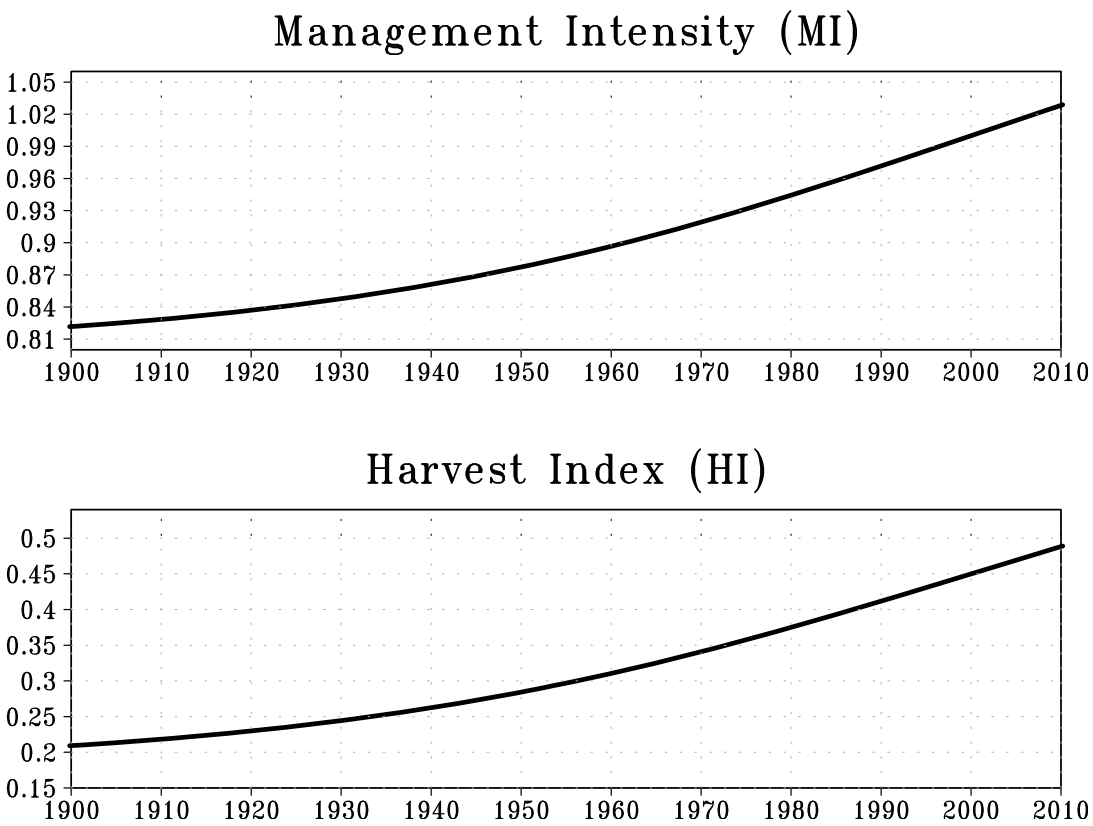

Extended Data Figure 1 | Management intensity (relative to year 2000) and harvest index change over time as used in the model. The analytical functions are hyperbolic tangent (see text). The parameter values correspond to a management intensity in 1961 that is 10% smaller than in 2010, and a harvest index of 0.31 in 1961 and 0.49 in 2010, based on literature review[34].

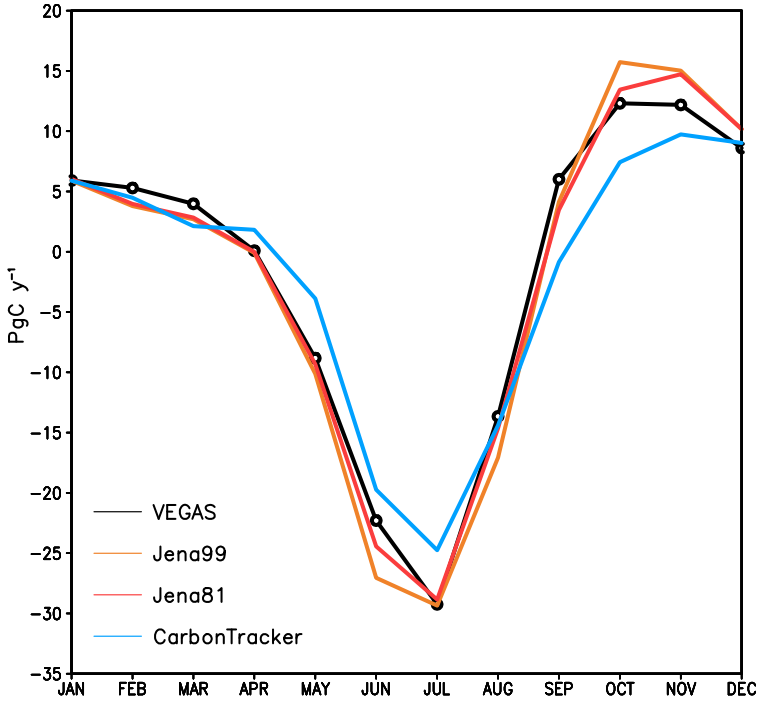

Extended Data Figure 2 | Average seasonal cycle of F_{TA}. F_{TA} (in Pg C yr^{-1}) for the period 2001–2010 from the VEGAS model, compared to atmospheric inversions of Jena81, Jena99 and CarbonTracker.

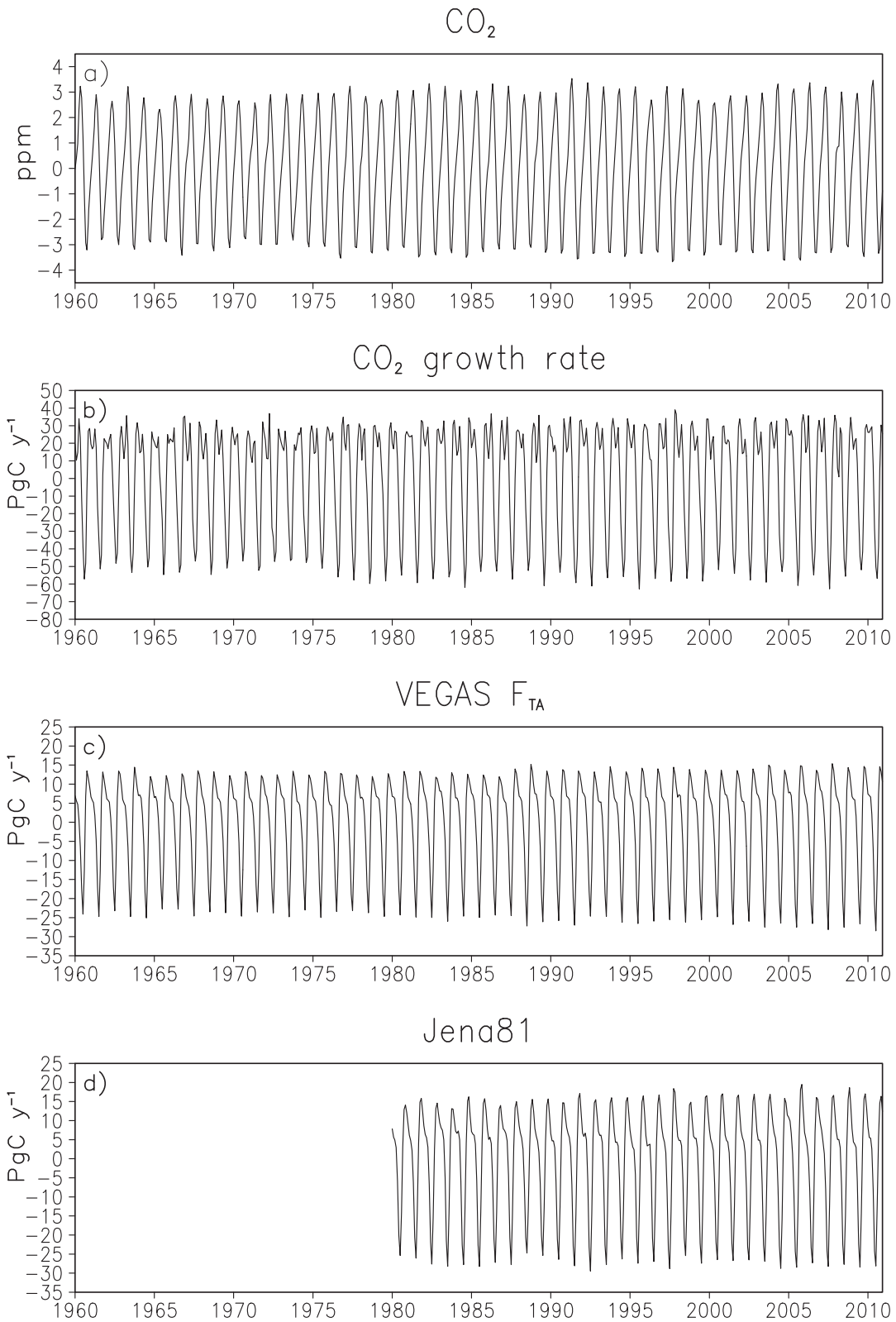

Extended Data Figure 3 | Time series analysis for seasonal cycles. **a**, Mauna Loa Observatory CO_2, in parts per million, p.p.m. **b**, Mauna Loa Observatory CO_2 growth rate, dCO_2/dt; **c**, F_{TA} from VEGAS; **d**, F_{TA} from the atmospheric inversion of Jena81. Trends and high-frequency variations have been removed following ref. 23. The seasonal amplitude in Figs 2 and 3 is calculated as the difference between the maximum and minimum F_{TA} each year.

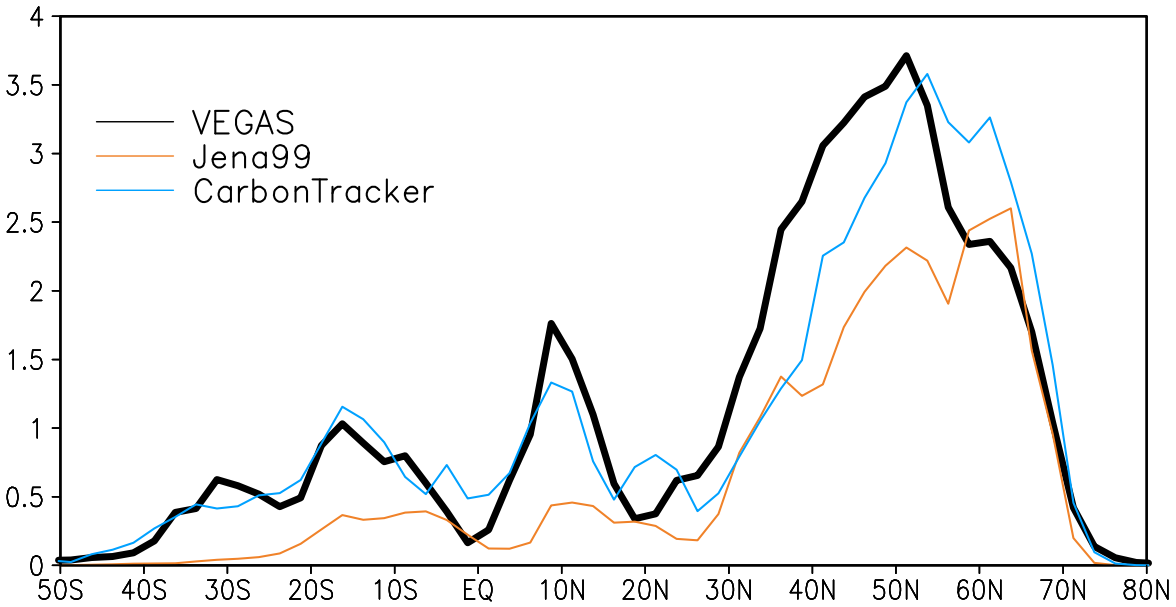

Extended Data Figure 4 | Latitude dependence of the seasonal amplitude of F_{TA}. Fluxes are summed over latitude bands for the VEGAS model and from two atmospheric CO_2 inversions: Jena99 and the CarbonTracker. The Northern Hemisphere mid-to-high-latitude region, driven by the winter–summer temperature contrast, is the main contributor. The Southern Hemisphere has the opposite phase to that of the Northern Hemisphere, but its contribution to the global total is small owing to its small land area. The two subtropical maxima around 10° N and 10° S are due to the wet–dry seasonal shift in the Inter-Tropical Convergence Zone (ITCZ) and monsoon movement; these are out of phase and largely cancel each other out in terms of their net contribution to the global total F_{TA} seasonal amplitude. The results are resampled into 2.5° latitude bands from the original resolutions of 0.5° × 0.5° for VEGAS, 5.0° × 5.0° for Jena99 and 1.0° × 1.0° for CarbonTracker.

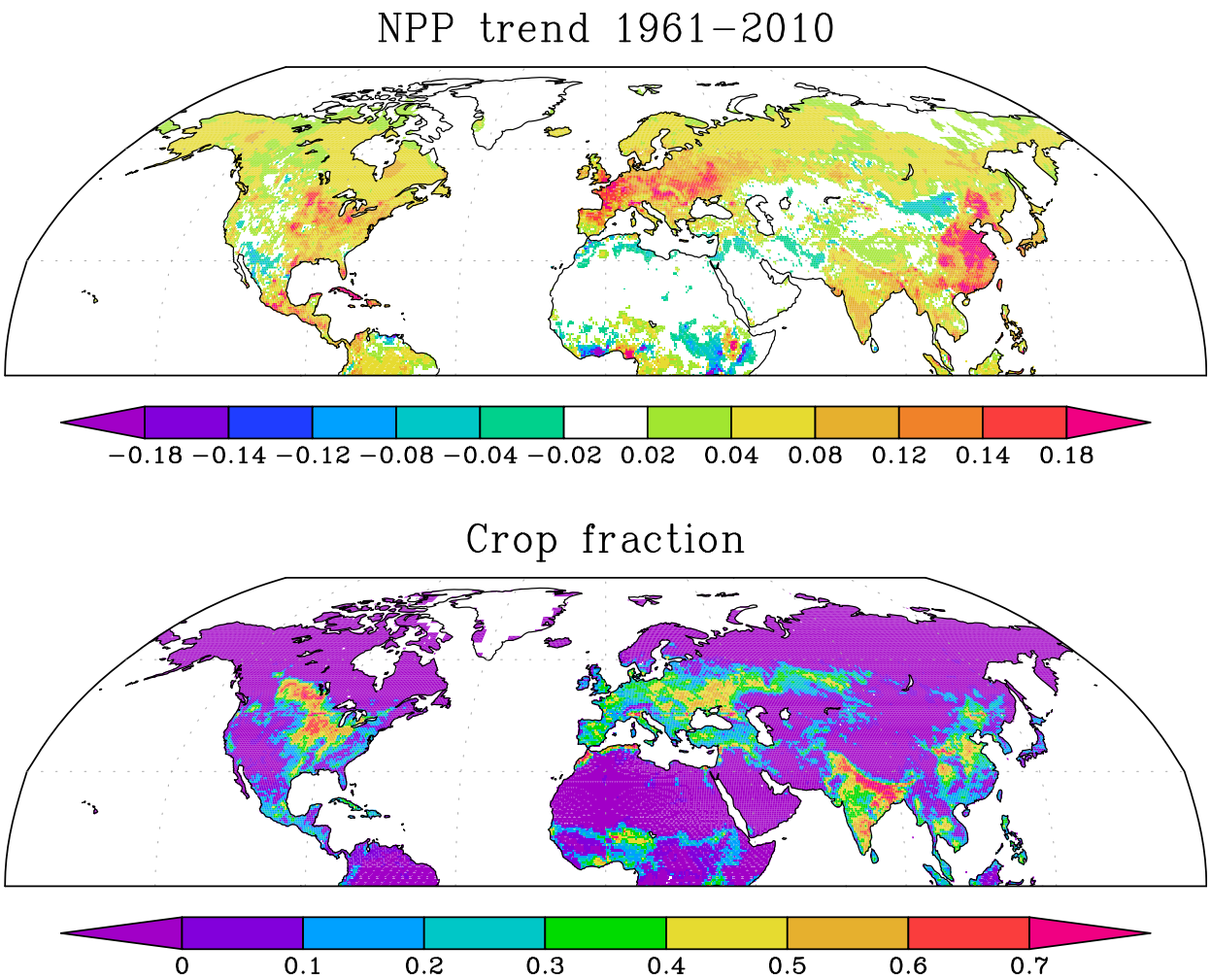

Extended Data Figure 5 | Trends in NPP. Modelled linear trends (in units of kg C m^{-2} over 50 years, upper panel) from 1961 to 2010 show major increases in the agricultural areas of North America, Europe and Asia (the lower panel shows the crop fraction in 2000). There are also widespread increases in much of the Northern Hemisphere, especially the high-latitude regions in response to warming and the CO_2 fertilization effect. Together, they are mostly responsible for the increase in F_{TA} and the CO_2 seasonal amplitude. Decreases in some regions are due to climate trends. Detailed regional patterns may not be well captured, for example, in the former Soviet Union, because of the simplified model representation of temporal changes.

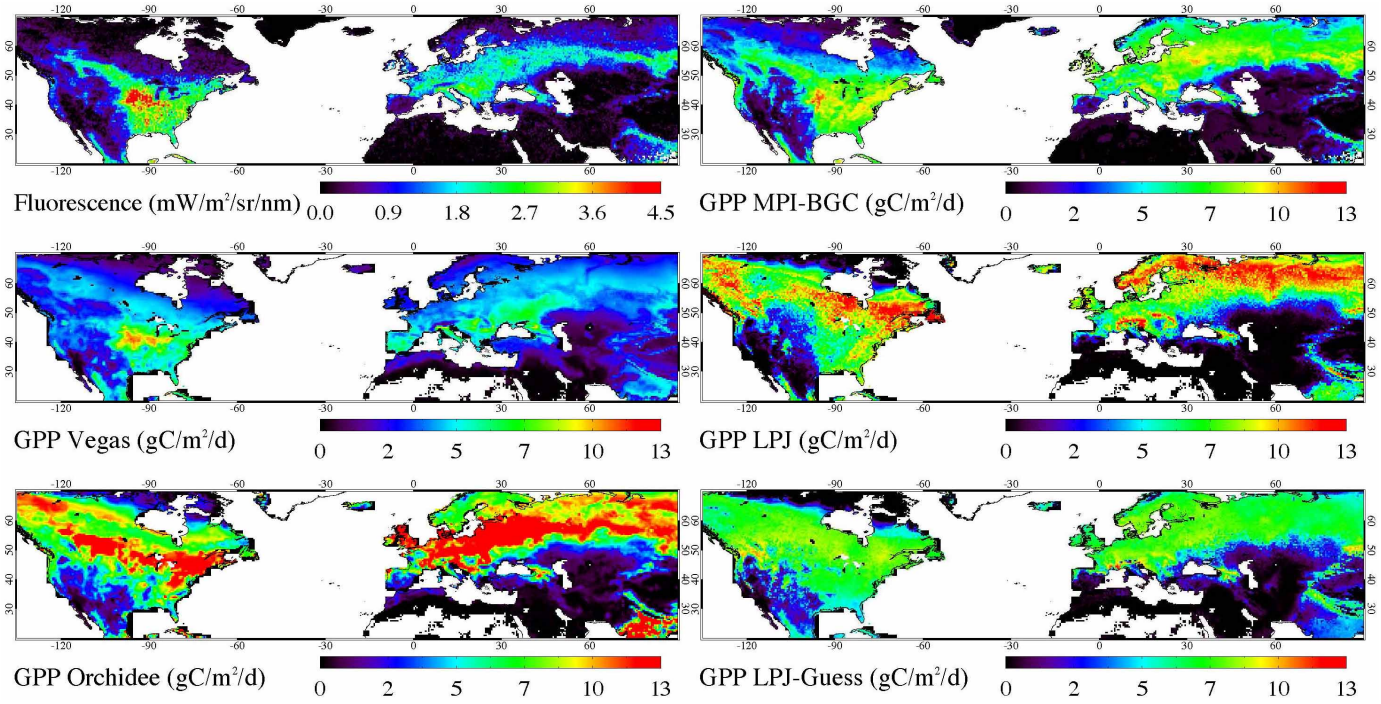

Extended Data Figure 6 | SIF. Measurements of SIF with the GOME-2 instrument on board the MetOp-A satellite platform are compared to GPP estimates from the data-driven model from MPI-BGC[35], and four mechanistic carbon cycle models (VEGAS, LPJ, Orchidee, and LPJ-Guess) from the TRENDY international project.

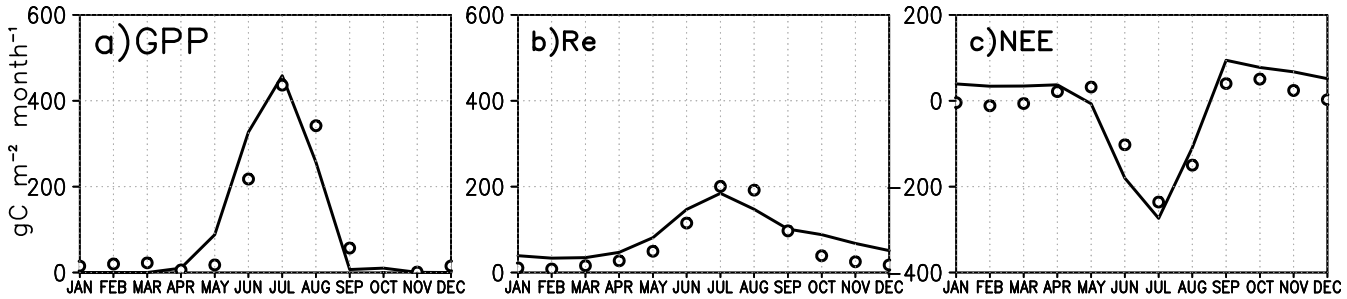

Extended Data Figure 7 | Model–data site validation. Comparison of VEGAS model (line) and FLUXNET observations (circles) at an agricultural site Bondville, Illinois (88.290398° W, 40.006199° N). **a**, GPP; **b**, R_e, **c**, NEE (= R_e minus GPP = F_{TA}). Shown are seasonal cycles averaged over the period 1996–2007.

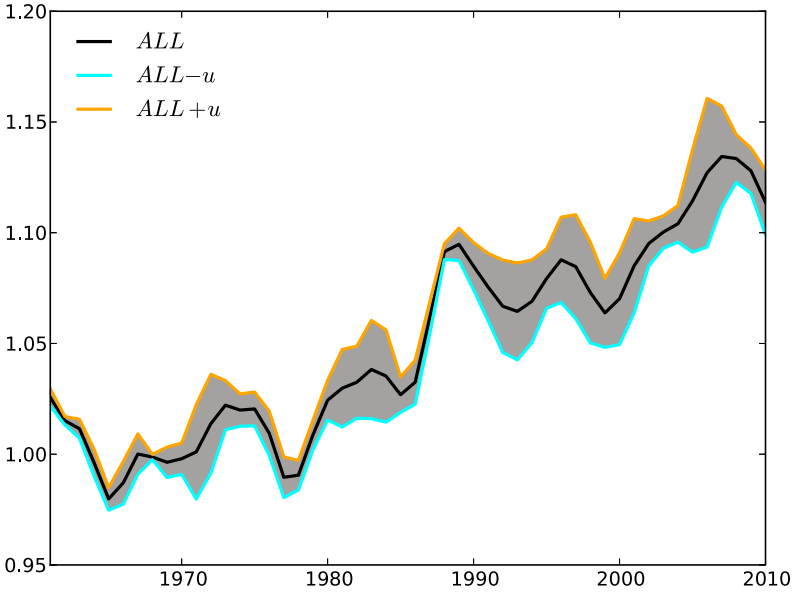

Extended Data Figure 8 | Uncertainty analysis. Uncertainties in the CO_2 seasonal amplitude trend due to model parametric errors in representing agricultural NPP. The upper and lower uncertainty range are labelled ALL + *u* and ALL − *u* respectively where *u* is uncertainty (standard deviation).

Extended Data Table 1 | Changes associated with the agricultural Green Revolution

	Population (billions)	Cropland area (million km^2)	Crop production (PgC y^{-1})	Harvest Index (HI)	Management Intensity (MI, relative to 2000)	Total production on cropland (PgC y^{-1})
1961	3	7.2	0.5 (0.6)	(0.31)	(0.9)	(4.0)
2010	7	8.7	1.5 (1.4)	(0.49)	(1.03)	(6.2)
Change 2010-1961	4	1.5	1.0 (0.8)	(0.18)	(0.13)	(2.2)
Percent change 2010-1961	130%	20%	200% (130%)	(60%)	(12%)	(55%)

This table summarizes the changes in population, cropland area, and crop production from 1961 to 2010 from FAO data and other statistics, and harvest index, management intensity and NPP_{crop} from the VEGAS model. Crop production refers to the harvested edible parts of crops, while NPP_{crop} is the total biomass production including above and below-ground biomass. All are measured in terms of carbon mass, which is typically about 50% of plant dry mass. Model results are in parentheses.

Extended Data Table 2 | The trend of CO_2 seasonal amplitude change from three model sensitivity experiments

	CLIM	CO2	LU	SUM	ALL
1961-2010 trend (% per year)	0.088	0.076	0.135	0.299	0.320
Percentage contribution to SUM	29%	26%	45%	100%	

Each experiment has only a single forcing of climate (CLIM) or CO_2 (CO2) or land use and management (LU) change. Their percentage contributions are in parentheses and the total is SUM. Additionally, the experiment ALL is the simulation with all three forcings as in Figs 2 and 3. The trend is calculated with a least-squares linear fit of the unsmoothed time series of seasonal amplitude of the modelled F_{TA}, and may be somewhat different from a visual inspection of Fig. 2, where the data has been smoothed to remove interannual variability.